

Supporting Information:

In-Situ Formation of Vanadium Nitride Quantum Dots on N-doped Carbon Hollow Spheres for Superior Lithium and Sodium Storage

Jun Yuan^{1,2+}, Xiang Hu²⁺, Junxiang Chen,² Yangjie Liu,² Taizhong Huang^{1*}, Zhenhai Wen^{2*}

¹ *Shandong Provincial Key Laboratory of Fluorine Chemistry and Chemical Engineering. University of Jinan, Jinan 250002, China*

² *CAS Key Laboratory of Design and Assembly of Functional Nanostructures, and Fujian Provincial Key Laboratory of Nanomaterials, Fujian Institute of Research on the Structure of Matter, Chinese Academy of Sciences, Fuzhou, Fujian 350002, China.*

[+] These authors contributed equally to this work.

[*] Corresponding authors

E-mail: chm_huangtz@ujn.edu.cn (T. Huang); and wen@fjirsm.ac.cn (Z. Wen)

Experimental

Chemicals Reagents: Ammonium metavanadate (NH_4VO_3 , analytic reagent) was purchased from Xin Weicheng Laboratory Equipment Co. LTD. And the Hydrochloric acid (HCl), hydrazine ($\text{N}_2\text{H}_4 \cdot \text{H}_2\text{O}$) were all analytic reagent. (Shanghai Chemical Reagents Co.) Dopamine hydrochloride and Tris buffer solution was purchased from Sinopharm Chemical Reagent Co. Ltd.

Preparation of the VOOH HSs precursor: VOOH HSs were prepared by a simple hydrothermal method reported previously.¹ The detailed synthesis process was as follows: ammonium metavanadate (NH_4VO_3) (0.2339g) was dissolved in 45 ml deionized water and form a transparent solution. Then 1ml of 1M HCl was added into the transparent solution in the rate of one drop per minute, and finally the color of the solution turned into diaphanous orange. After that, 2ml hydrazine ($\text{N}_2\text{H}_4 \cdot \text{H}_2\text{O}$) was introduced into the orange diaphanous solution and stirred strongly for 10 minutes. Then the diaphanous solution became turbid and gradually transformed into a gray suspension solution. Afterwards, the suspension solution was sealed in a 50 ml Teflon-lined autoclave and hydrothermally treated at 120 °C for 8 hours. In the end, after the autoclave cooled to room temperature, the precipitate of the solution was collected by centrifugation and washed with the mixture of deionized water and ethanol to remove the impurities. The collected precipitate was fully dried in vacuum at 60 °C for the next process.

Preparation of the VNQD@NC HSs, VN@NC nanoparticles (NPs), VN-bulk NPs:

The as-prepared VOOH HSs (150 mg) was dispersed into the Tris buffer solution (100

ml), and then stirred strongly for 20 minutes. Afterwards, 100 mg of Dopamine hydrochloride was added into the suspension solution and stirred for 24 hours at room temperature. Finally, the carbon-coated VOOH HSs was collected by centrifugation and thoroughly washed with the deionized water. After drying in a vacuum at 60 °C, the hydroxyoxyvanadium@N-doped carbon hollow spheres (VOOH@NC HSs) was formed. The solid VOOH@NC HSs was annealed at 650 °C for 2 hours in a NH₃ atmosphere to prepare the VNQD@NC HSs. As comparison, the VN-bulk NPs were obtained by a direct nitridation of the VOOH HSs, and VN@NC NPs were generated via a carbon-encapsulated process of the VN-bulk NPs and then carbonated at 650 °C in Ar₂ atmosphere, which is similar to the above mentioned process of synthesizing VNQD@NC HSs.

Materials Characterization: The X-ray diffraction (XRD) measurements were performed using a Miniflex 600 powder X-ray diffractometer equipped with Cu K α radiation in the 2 θ range from 10° to 80° with the scanning speed of 0.05° s⁻¹. The morphology and microstructure of the materials were characterized by using field emission scanning electron microscopy (FESEM) (Hitachi SU-8020), transmission electron microscopy (TEM), and high resolution TEM (HRTEM) (Tecnai F20) tests. Energy dispersive X-ray spectroscopy analysis was implemented in the FESEM and TEM tests. The amount of carbon content of the materials was examined by using thermal gravimetric (TG) analysis (Netzsch STA449F3) in air atmosphere with a heating rate of 10 °C min⁻¹ from room temperature to 800 °C. Nitrogen adsorption–desorption isotherms and Brunauer–Emmett–Teller (BET) surface area

tests were conducted by a self-acting gas sorption analyzer (Hiden IGA100B). The measurements were conducted at 77 K, and the pore-size distribution was obtained, simultaneously. The elemental electron states of each material were identified by using the X-ray photoelectron spectrometer (XPS) (ESCALAB 250).

Electrochemical measurements: The anode was constituted by compressing a slurry of the active material powder 80 wt%, conductive carbon (super P) 10 wt% and binder (sodium carboxymethyl cellulose, CMC) 10 wt% in deionized water onto a copper foil with the diameter of 12 mm. The electrode plate was dried at 60 °C in vacuum for 24 hours. The loading mass of active material in electrode is in the range of 1 to 1.5 mg cm⁻². And the 2032 type coin cells were assembled into a half-battery in an argon-filled glove box where the concentrations of moisture and oxygen were both below 1 ppm. Lithium metal (sodium metal for sodium batteries), was used as the cathode electrode, and 1 M LiPF₆ dissolved in 1:1 (vol/vol) mixture of ethylene carbonate (EC) and dimethyl carbonate (DC) as the electrolyte. And the 1 M NaPF₆ dissolved in 1:1 (vol/vol) mixture of ethylene carbonate (EC) and dimethyl carbonate (DC) with 5% fluoroethylene carbonate as the electrolyte for sodium batteries. The separator was a polypropylene microporous film and a whatman glass microfiber was adopted for sodium batteries. The galvanostatic charge-discharge tests were measured by the LAND battery testers (Wuhan Kingnuo Electronic Co., China) at varied current densities at room temperature in the potential window between 0.01 and 3.0 V. Cyclic voltammetry (CV) measurements were conducted by using a CHI 660E electrochemical workstation at the scanning rate of 0.1 mV s⁻¹. For LIBs, the cell was first activated at

0.1 A g⁻¹ for first three cycles and then the CV tests were conducted with a higher current density for the long-time cycling tests. Electrochemical impedance spectroscopy (EIS) test was also performed by using a CHI 660E electrochemical workstation within the frequency range from 10 mHz to 100 kHz.

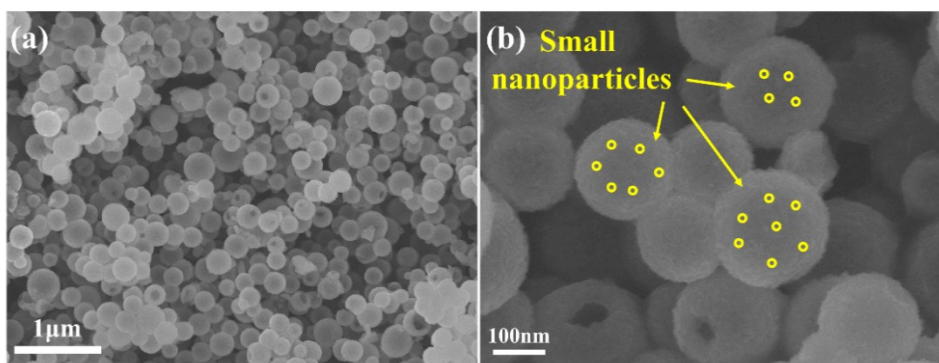


Figure S1. (a, b) FESEM images of VOOH.

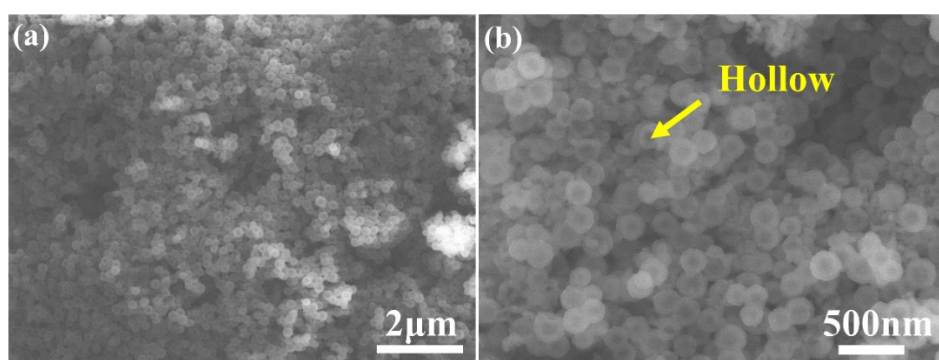


Figure S2. (a,b) FESEM images of VOOH@NC.

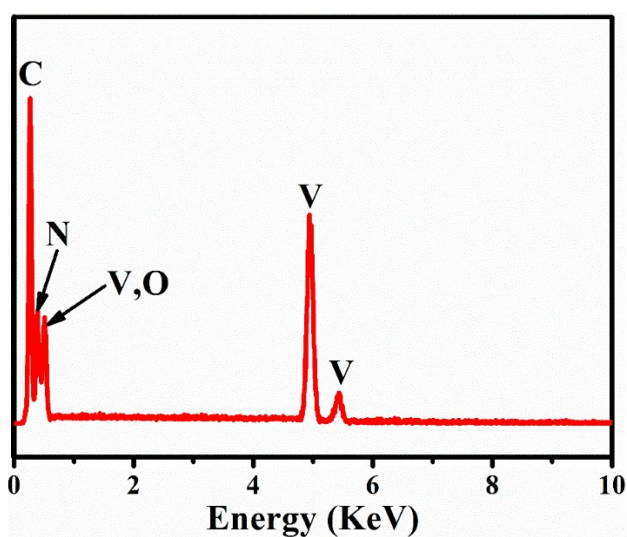


Figure S3. The energy dispersive X-ray spectroscopy of the VNQD@NC HSs.

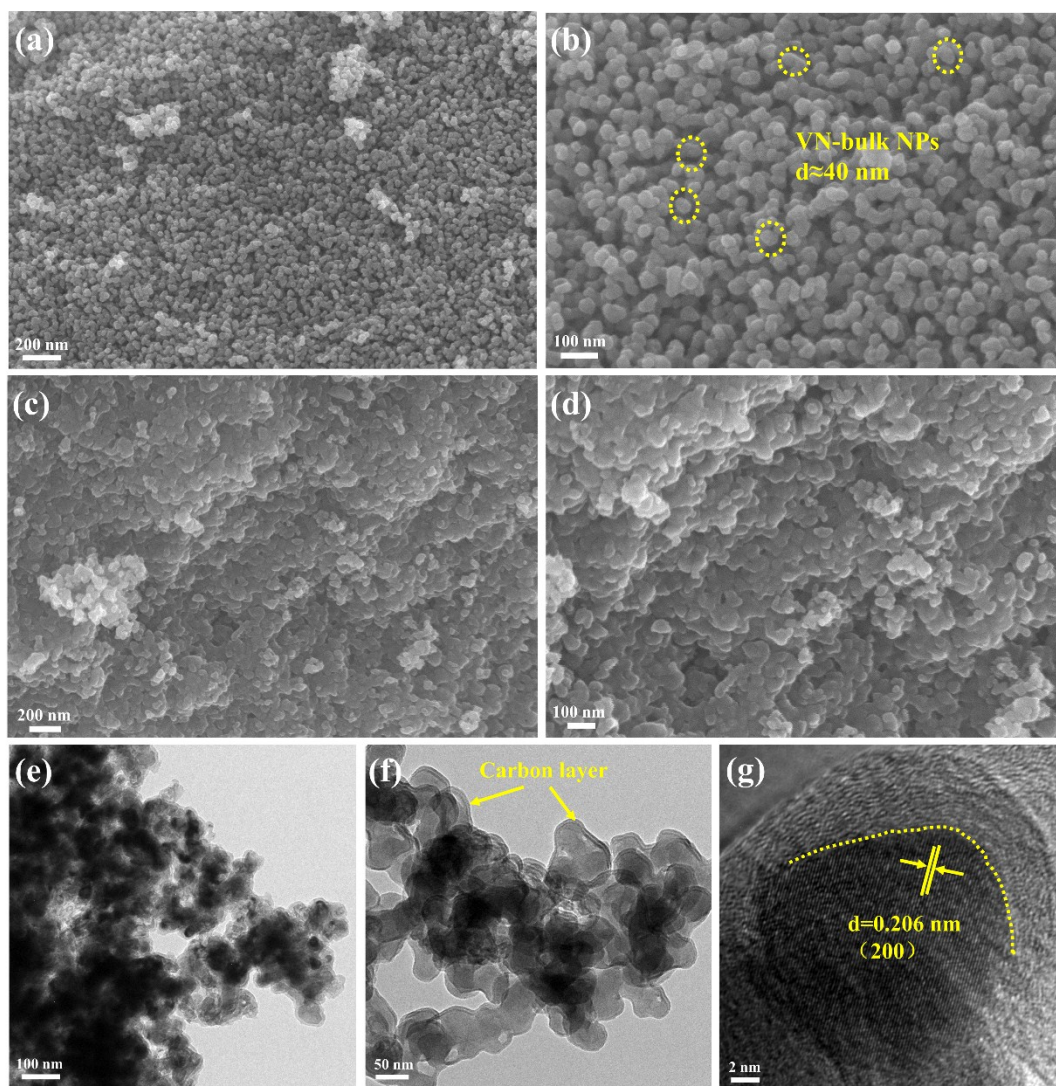


Figure S4. (a,b) FESEM images of VN-bulk NPs. (c,d) FESEM images, (e, f) TEM images, and (g) HRTEM image of VN@NC NPs.

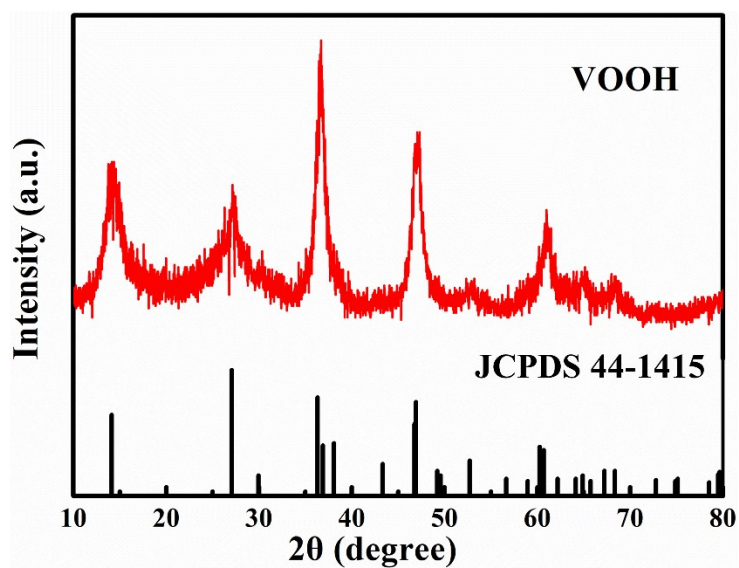


Figure S5. XRD patterns of the VOOH HSs

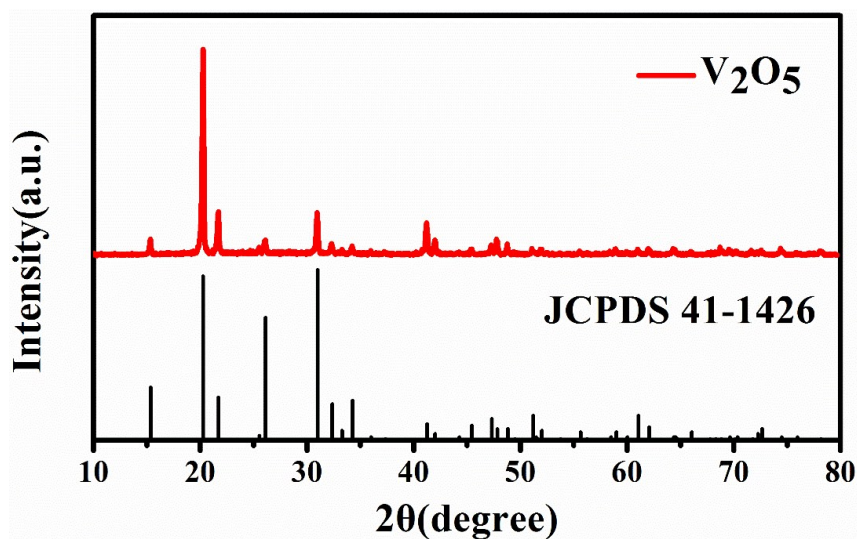


Figure S6. XRD patterns of the final product after TGA measurement.

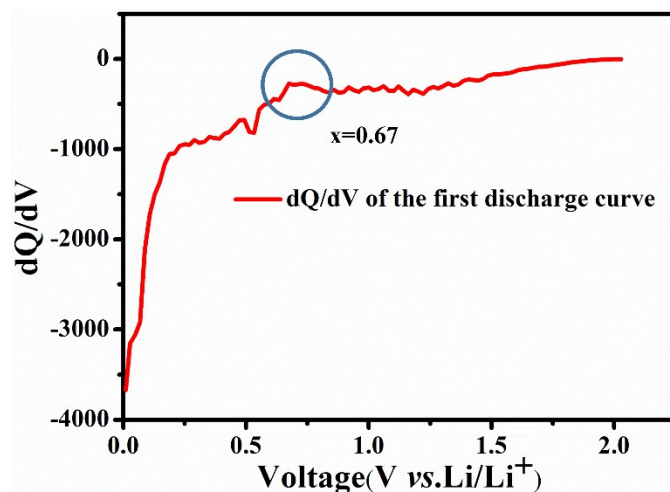


Figure S7. The dQ/dV plots of the first discharge curve in Figure 3b.

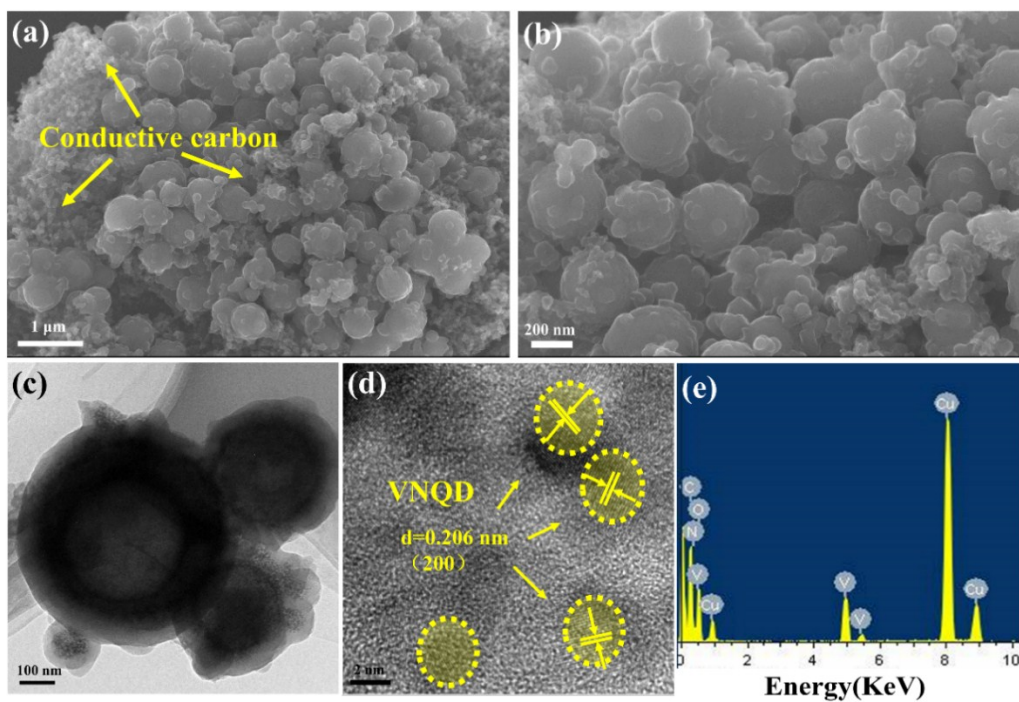


Figure S8. (a,b) FESEM images, (c) TEM image, (d) HRTEM image, and (e) EDS spectrum of VNQD@NC HSs at a current density of 0.1 A g^{-1} for LIBs after 200 cycles.

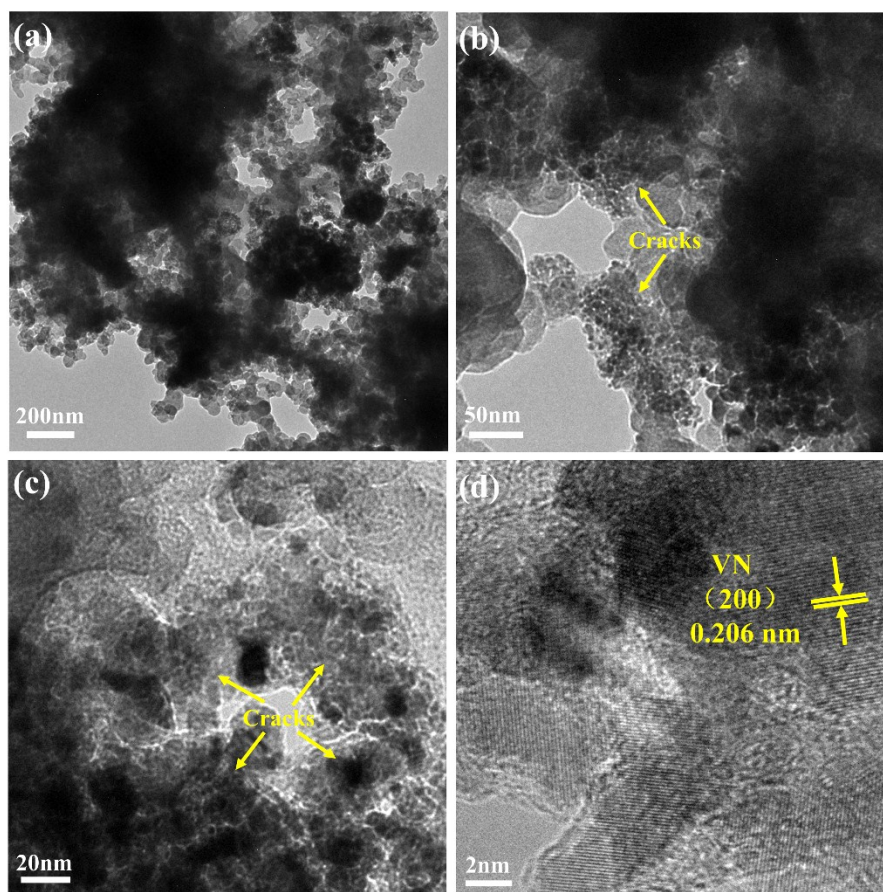


Figure S9. (a-d) TEM images of VN@NC NPs at a current density of 0.1 A g^{-1} for LIBs after 200 cycles.

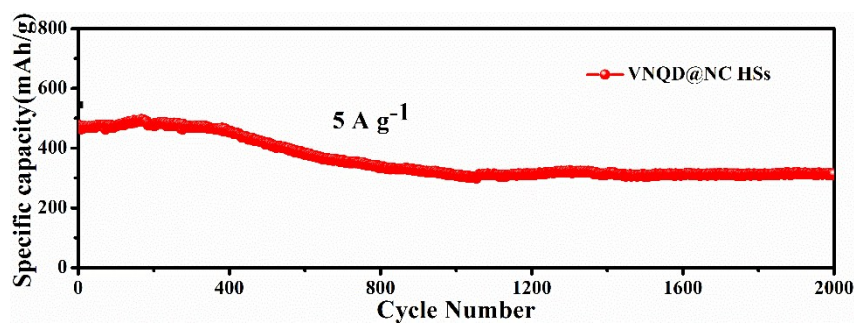


Figure S10. Cycling performance of VNQD@NC HSs at the current density of 5 A g^{-1} for LIBs.

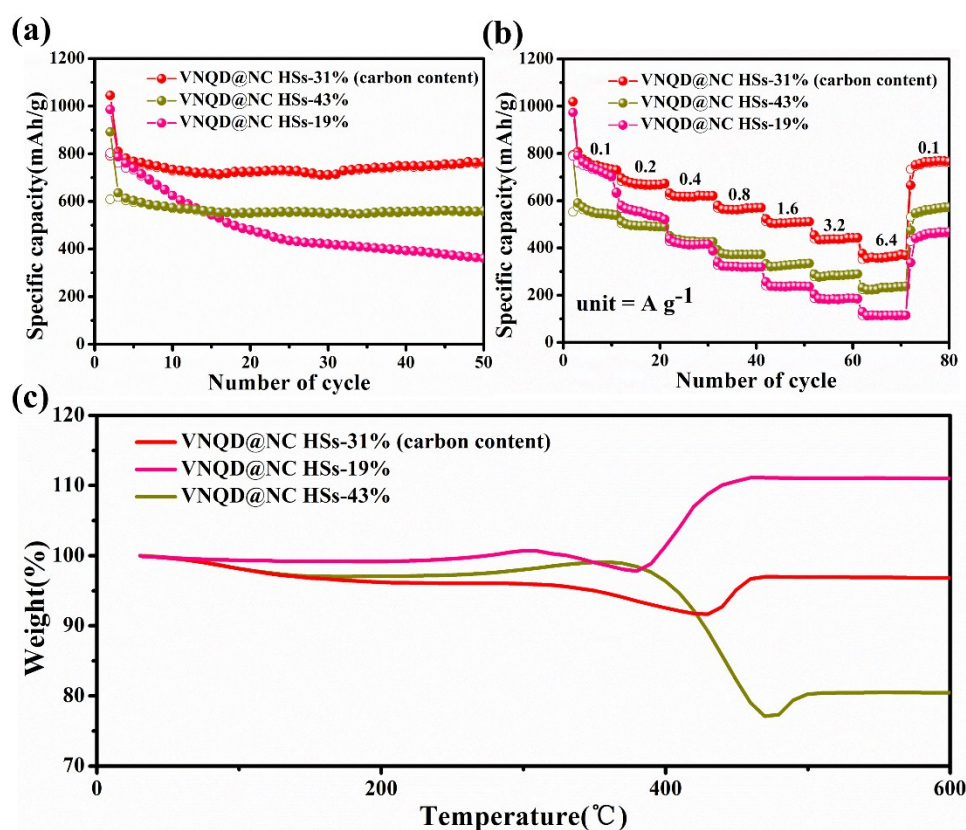


Figure S11. (a) Cycling performance of VN@NC HSs with various carbon contents at the current density of 0.1 A g⁻¹ for LIBs. (b) Rate capability and (c) TG curves of VNQD@NC HSs with various carbon contents.

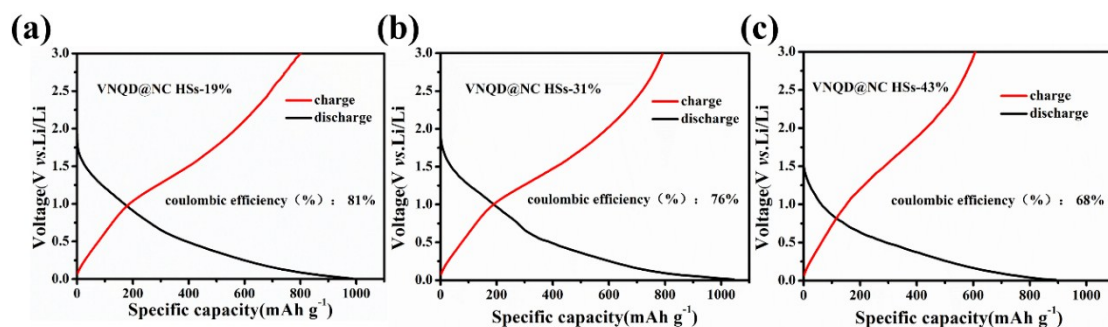


Figure S12. The initial charge-discharge Voltage profiles of (a) VNQD@NC HSs-19%, (b) VNQD@NC HSs-31% and (c) VNQD@NC HSs-43% at the current density of 0.1 A g⁻¹ for LIBs.

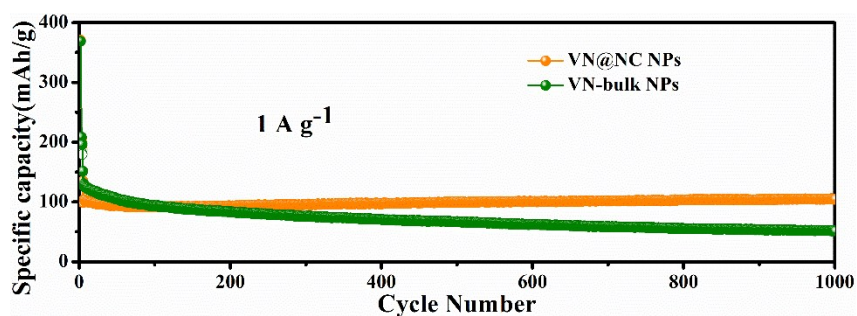


Figure S13. Cycling performance of VN@NC NPs and VN-bulk NPs at the current density of 1 A g^{-1} for SIBs.

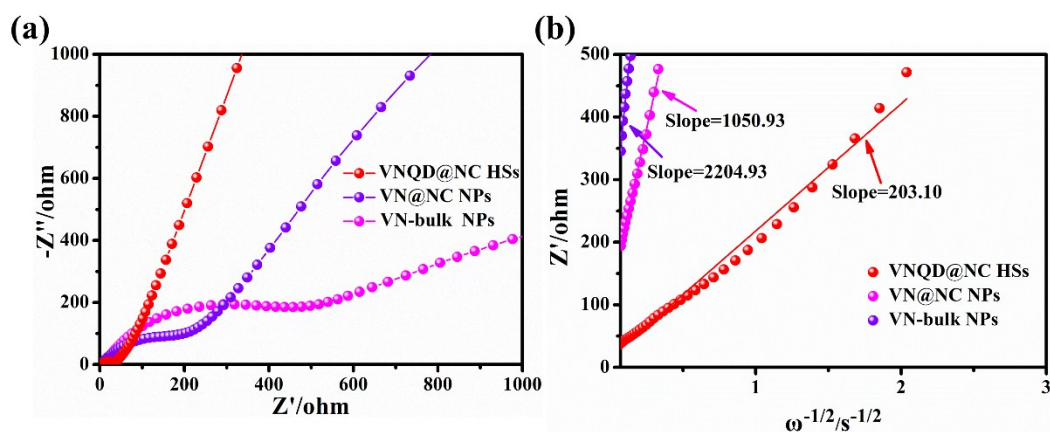


Figure S14. (a) Nyquist plots of the VNQD@NC HSs, VN@NC NPs and VN-bulk NPs electrode after 200 cycles at a current density of 0.1 A g^{-1} for sodium-ion batteries. (b) Relation of Z' - $\omega^{-1/2}$ curves of VNQD@NC HSs, VN@NC NPs and VN-bulk NPs in the low-frequency region for sodium-ion batteries.

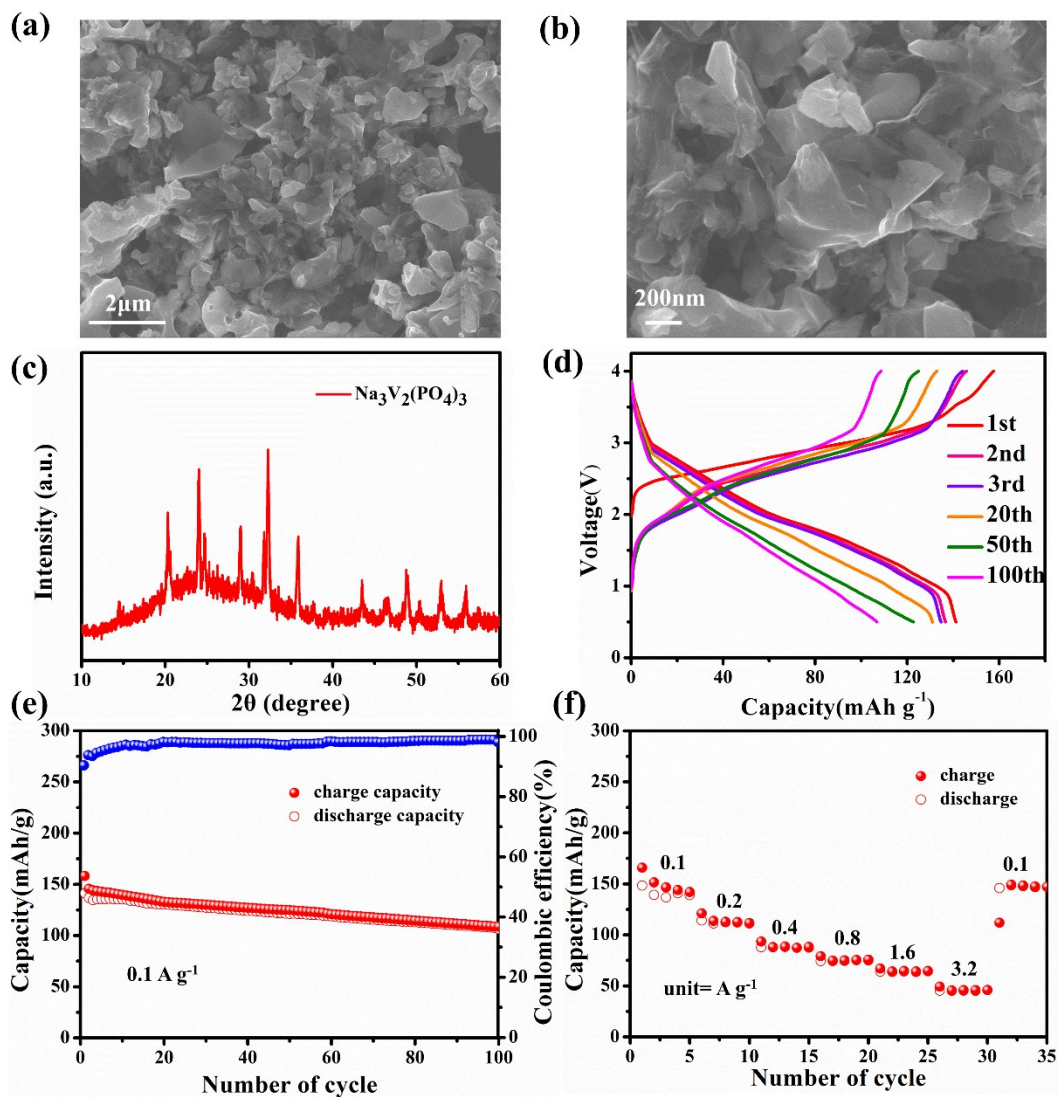


Figure S15. (a, b) FESEM images and (c) XRD pattern of $\text{Na}_3\text{V}_2(\text{PO}_4)_3$. (d) Charge and discharge curves of NVP||VNQD@NC HSs full cell at 0.1A g^{-1} . (e) Cycle and (f) rate performance of the full cell.

Table S1. Electrochemical performance comparison of VNQD@NC HSs with various nitride electrodes for LIBs applications.

Sample	Current density (A g⁻¹)	Cycling number	Specific capacity (mAh g⁻¹)	References
VNQD@NC HSs	0.1	200	830	This work
VN HS	0.05	40	720	2
VN -carbon	0.065	100	320	3
VN nanosheet	0.1	100	520	4
Fe₃N@C	0.1	500	370	5
Cu₃N	1	150	275	6
MoN-GNS-30%	0.1	100	518	7
FeN@RGO	0.1	100	400	8
FeCoN/N-rG-O	0.1	60	520	8
Zn₃N₂	0.023	1	555	9
Ni_{0.33}Co_{0.67}N	0.5	50	350	10
Mn₃N₂	0.08	110	463	11
TiN	0.335	100	450	12
G/TiN	0.02	200	554	13

Table S2. Electrochemical performance comparison of VNQD@NC HSs with various nitride electrodes for SIBs applications.

Sample	Current density (A g⁻¹)	Cycling number	Specific capacity (mAh g⁻¹)	References
VNQD@NC HSs	0.1	200	360	This work
	1	1400	315	
VNQD-500	1.2	800	254	14
Mn_{0.33}Co_{0.67}N	0.5	90	277	15
Por-Mo₂N-NBS	0.1	200	180	16
NiN	0.211	30	170	17
Sn₃N₄	0.05	50	240	18
Fe₂N@C	0.5	1000	75	19
Fe₃N@C	0.4	300	280	20

References

1. Wu, C.; Zhang, X.; Ning, B.; Yang, J.; Xie, Y., *Inorg. Chem.*, 2009, **48**, 6044-6054.
2. Zhao, D.; Cui, Z.; Wang, S.; Qin, J.; Cao, M., *J. Mater. Chem. A*, 2016, **4**, 7914-7923.
3. Kundu, D.; Krumeich, F.; Fotedar, R.; Nesper, R., *J. Power Sources*, 2015, **278**, 608-613.
4. Peng, X.; Li, W.; Wang, L.; Hu, L.; Jin, W.; Gao, A.; Zhang, X.; Huo, K.; Chu, P. K., *Electrochimica Acta*, 2016, **214**, 201-207.
5. Huang, H.; Gao, S.; Wu, A.-M.; Cheng, K.; Li, X.-N.; Gao, X.-X.; Zhao, J.-J.; Dong, X.-L.; Cao, G.-Z., *Nano Energy*, 2017, **31**, 74-83.
6. Deshmukh, R.; Zeng, G.; Tervoort, E.; Staniuk, M.; Wood, D.; Niederberger, M., *Chem. Mater.*, 2015, **27**, 8282-8288.
7. Zhang, B.; Cui, G.; Zhang, K.; Zhang, L.; Han, P.; Dong, S., *Electrochimica Acta*, 2014, **150**, 15-22.
8. Lai, L.; Zhu, J.; Li, B.; Zhen, Y.; Shen, Z.; Yan, Q.; Lin, J., *Electrochimica Acta*, 2014, **134**, 28-34.
9. Pereira, N.; Klein, L. C.; Amatucci, G. G., *J. Electrochem. Soc.*, 2002, **149**, A262.
10. Das, B.; Reddy, M. V.; Chowdari, B. V., *Nanoscale*, 2013, **5**, 1961-1966.
11. Sun, Q.; Fu, Z.-W., *Appl. Surf. Sci.*, 2012, **258**, 3197-3201.
12. Balogun, M.-S.; Yu, M.; Li, C.; Zhai, T.; Liu, Y.; Lu, X.; Tong, Y., *J. Mater. Chem. A*, 2014, **2**, 10825-10829.
13. Yue, Y.; Han, P.; He, X.; Zhang, K.; Liu, Z.; Zhang, C.; Dong, S.; Gu, L.; Cui, G.,

J. Mater. Chem., 2012, **22**, 4938.

14. Wang, L.; Sun, J.; Song, R.; Yang, S.; Song, H., *Adv. Energy Mater.*, 2016, **6**, 1502067.

15. Zhu, L.; Chen, Z.; Song, Y.; Wang, P.; Jiang, Y.; Jiang, L.; Zhou, Y. N.; Hu, L., *Nanoscale*, 2018, **10**, 5581-5590.

16. Liu, S.-L.; Huang, J.; Liu, J.; Lei, M.; Min, J.; Li, S.; Liu, G., *Mater. Lett.*, 2016, **172**, 56-59.

17. Li, X. J.; Hasan, M. M.; Hector, A. L.; Owen, J. R., *J. Mater. Chem. A*, 2013, **1**, 6441-6445.

18. Li, X.; Hector, A. L.; Owen, J. R.; Shah, S. I. U., *J. Mater. Chem. A*, 2016, **4**, 5081-5087.

19. Liu, S.; Liu, J.; Wang, W.; Yang, L.; Zhu, K.; Wang, H., *RSC Adv.*, 2016, **6**, 86131-86136.

20. Li, Z.; Fang, Y.; Zhang, J.; Lou, X. W. D., *Adv. Mater.*, 2018, **30**, 1800525.